Ultrasonics Sonochemistry 95 (2023) 106415

Contents lists available at ScienceDirect

Ultrasonics Sonochemistry

journal homepage: www.elsevier.com/locate/ultson

Effect of ultrasound power on HCl leaching kinetics of impurity removal of aphanitic graphite

Xiangning Bu [a,*], Zheng Tong [a], Muhammad Bilal [b], Xibing Ren [a], Mengqian Ni [a], Chao Ni [a], Guangyuan Xie [a]

[a] Key Laboratory of Coal Processing and Efficient Utilization (Ministry of Education), School of Chemical Engineering and Technology, China University of Mining & Technology, Xuzhou 221116, China

[b] Department of Mining Engineering, Balochistan University of Information Technology, Engineering and Management Sciences (BUITEMS), Quetta, Pakistan

ARTICLE INFO

Keywords:
Aphanitic graphite
Ultrasound
Leaching kinetics
Ash impurity removal
HCl

ABSTRACT

This study aimed to investigate the effect of ultrasonic power and temperature on the impurity removal rate during conventional and ultrasonic-assisted leaching of aphanitic graphite. The results showed that the ash removal rate increased gradually (~50 %) with the increase in ultrasonic power and temperature but deteriorated at high power and temperature. The unreacted shrinkage core model was found to fit the experimental results better than other models. The Arrhenius equation was used to calculate the finger front factor and activation energy under different ultrasonic power conditions. The ultrasonic leaching process was significantly influenced by temperature, and the enhancement of the leaching reaction rate constant by ultrasound was mainly reflected in the increase of the pre-exponential factor A. Ultrasound treatment improved the efficiency of impurity mineral removal by destroying the inert layer formed on the graphite surface, promoting particle fragmentation, and generating oxidation radicals. The poor reactivity of hydrochloric acid with quartz and some silicate minerals is a bottleneck limiting the further improvement of impurity removal efficiency in ultrasound-assisted aphanitic graphite. Finally, the study suggests that introducing fluoride salts may be a promising method for deep impurity removal in the ultrasound-assisted hydrochloric acid leaching process of aphanitic graphite.

1. Introduction

The most common applications of graphite include electrodes of batteries/storage (34 %), refractories (20 %), lubricants (6 %), foundries (5 %), batteries (4 %), graphite shapes (4 %), recarburizing (1 %), and others (24 %) [1,2]. With an estimated 65 % share of global production in 2022, China emerged as the world's largest graphite producer. The majority of China's graphite output was in the form of flake graphite, which accounted for about 76 % of the production, while aphanitic graphite made up around 24 % [3]. It is anticipated that China's reserves of graphite will be depleted within the next two decades [4]. The purification and enrichment of aphanitic graphite have become a subject of growing interest due to the ongoing consumption of flake graphite with superior washability [1,5–7]. Graphite beneficiation is primarily achieved through flotation (using various reagents, both conventional and column flotation) and leaching (which includes chemical leaching, roasting and leaching, and microwave methods) [1,8,9]. Ultrasound treatment shows promise for achieving better flotation results in mineral processing when compared to conventional flotation methods [10–14]. This is due to its ability to eliminate slime coating, remove oxidation films, aid in desulfuration, generate tiny bubbles, disperse flotation reagents, and facilitate aggregation [15]. The use of ultrasound treatment in graphite flotation is beneficial due to its ability to micro-scrub loosely-bound ash impurities from the graphite surface and break down graphite-impurity aggregates. This results in improved efficiency in the flotation process, as it promotes more effective interactions between the graphite flakes and the collector [16]. In addition to removing impurities from the surface of graphite, ultrasonic treatment has the added benefit of reducing the size of flaky graphite. This in turn can help to expedite the graphite flotation cleaning process [17]. Nanobubbles can be generated by ultrasound cavitation, which is an important factor in the flotation process [9,15,18–21]. Although the use of ultrasound treatment in graphite flotation did not result in the production of nanobubbles, it is worth noting that advanced flotation techniques can still be used to upgrade fine graphite to a carbon content of around 95 %. However, further upgrading of the graphite through physical methods

* Corresponding author.
E-mail address: xiangning.bu@foxmail.com (X. Bu).

https://doi.org/10.1016/j.ultsonch.2023.106415
Received 29 January 2023; Received in revised form 11 April 2023; Accepted 17 April 2023
Available online 20 April 2023

Table 1
Summary of the literature on ultrasound-assisted leaching processes of graphite.

Objective	Main findings	Ref.
Solvent leaching of sodium and potassium from coal	Ultrasound significantly reduced the processing time of alkali removal from coal. An intermediate frequency of 360 kHz proved to be ideal for alkali removal due to the optimal combination of cavitation and streaming effects. The shrinking core model gives the best fit for surface diffusion-controlled reactions.	[36]
Demineralization of coal	The ultrasound can produce higher demineralization and desulphurization efficiency by enhancing the particle surface area and extractability of coal impurities at the minimum consumption of time, reagent, and energy.	[47]
Sulfurization of coal	The dual-frequency system is optimal for sulfur removal due to the simultaneous presence of cavitation and streaming effects. In almost all cases, sulfate-sulfur removal is more than 90 %, as observed in aqueous-based ultrasonic de-sulfurization.	[48]
Leaching alkali elements from coals	Removal efficiencies for ultrasonic chemical washing are significantly higher than that of stirring. Ultrasound-assisted chemical washing may be employed in a coal-fired power plant to contain the severity of fouling deposits.	[49]
Dissolution of uranium from graphite substrate	Comparison with silent conditions revealed that an enhanced rate was obtained due to the use of ultrasound under optimum conditions.	[50]

Note: As coals have similar properties to a certain, the published papers on the leaching of coals were also summarized.

remains a challenging task [7,8,22,23].

Chemical purification through leaching is the most common technique to produce high-purity graphite after flotation [1,8]. The chemical purification methods of graphite mainly include the acid-base method, hydrofluoric acid method, chloride roasting method, and high-temperature purification method [8]. Compared with high-temperature treatment, direct acid leaching treatment has the characteristics of low energy consumption and low air pollution. However, the acid leaching method also faces the problem of low impurity removal efficiency. An acid-base method was found to be capable of producing aphanitic graphite concentrate with a fixed carbon content of 90.88 % during the 7-hour reaction period [24]. Liu and Gao [25] used the alkali fusion-acid leaching method to increase the fixed carbon content of aphanitic graphite from 82.67 % to 93.42 % with 3 h of calcination time and 3 h of leaching time. Wang, et al. [26] increased the carbon content of aphanitic graphite from 90.20 % to 99.00 % by combining alkali roasting (1 h roasting time) and acid leaching process (2 h leching time). Kaya and Canbazoğlu [27] reported that the fixed carbon content of graphite can be increased by ~ 60 % with 20 % HCl + 4 % HF and 4 h of leaching time. Hong, et al. [28] increased the purity of aphanitic graphite from 87.8 % to 99.1 % by an HCl-HF system after a 4 h reaction time. Tang, et al. [29] purified aphanitic graphite using a one-step HF-HCl mixed acid method, and the fixed carbon content of aphanitic graphite was increased from 83.08 % to 99.41 % with a 3 h leaching time. Zaghib, et al. [30] increased the fixed carbon content of graphite from 98.5 % to 99.9 %30 % using H_2SO_4 + 30 % NH_xF_y system. Xie, et al. [31] used hydrochloric acid-sodium fluoride for the removal of aphanitic graphite, and the fixed carbon content of aphanitic graphite could be increased from 83.08 % to 98.37 %. The hydrochloric acid-sodium fluoride method is highly effective in treating aphanitic graphite ore without altering its surface morphology or crystal structure. High-temperature roasting pretreatment can significantly improve the reactivity of impurities in aphanitic graphite, but there are shortcomings such as high energy consumption, low purification efficiency, serious equipment losses, and high loss of valuable minerals.

The ultrasound-assisted techniques have been widely used to enhance the efficiency of metal leaching from ores and waste materials [32]. The mechanisms of ultrasound-assisted leaching can be attributed to the enhancement of mineral solubility mechanisms and transport phenomena [33]. The physical and chemical effects induced by ultrasound cavitation can improve transportation rates, enhance the surface area and ease leachants penetration rate into the matrix, remove and slow down the generation of the diffusion layer on the particle surface, and promote the solid–liquid reaction (the generated free radicals) [32,34,35]. The related studies on the ultrasound-assisted leaching of graphite and coal are summarized in Table 1. It is demonstrated that ultrasound treatment can enhance the leaching efficiency of alkali elements from coal and the dissolution of uranium from graphite substrate. Compared to conventional leaching, the ultrasound-assisted process can significantly shorten the processing time. In particular, Srivalli and Nagarajan [36] investigated the leaching kinetics of ultrasound-assisted solvent leaching of sodium and potassium from coal. They found that the shrinking core model gives the best fit for surface diffusion-controlled reactions. In addition, various researchers have evaluated the ultrasound-assisted leaching kinetics of other metals. Rahimi, et al. [37] reported that ash mass diffusion was the controlling step of the overall reaction kinetics for the leaching vanadium from fly ash. The research conducted by Turan, et al. [38] revealed that the dissolution kinetics of blended copper slag using ultrasound-assisted techniques were found to be influenced by different kinetic models depending on the leaching parameters, owing to the utilization of two distinct chemical reactants, hydrogen peroxide, and acetic acid. Li, et al. [39] found that the ultrasound-assisted leaching of iron from boron carbide waste scrap fits chemical reaction-controlled model, diffusion-controlled model for the first stage and second stage, respectively. Zhang, et al. [40] showed that the ultrasound-assisted leaching of potassium from phosphorus-potassium associated ore follows the classical unreacted-core shrinking model with internal diffusion being the rate-limiting step. Avvaru, et al. [41] indicated that the leaching operation of uranium can be explained as a classical shrinking core kinetics phenomenon with pore diffusion resistance as the rate-limiting step. According to He, et al. [42], the semi-empirical Averami equation was shown to be an effective model for describing the extraction kinetics of Mn, which became more diffusion-controlled after mechanical activation, as revealed by the modeling results. Gui, et al. [43] reported that the internal diffusion step controlled the ultrasound-assisted leaching process of gold. The increase in the ultrasound-assisted leaching rate is due to the decrease of activation energy from 22.65 kJ/mol to 13.86 kJ/mol. demonstrated that the classical shrinking core model was applicable for both conventional and ultrasound-assisted leaching. Further, the rate-controlling mechanism for both techniques was found to be a combination of product layer diffusion and chemical reactions at the chalcopyrite surface. Ma, et al. [44] revealed that the leaching kinetics of K-feldspar with and without ultrasound can be successfully modeled by a classic shrinking core model with the product layer diffusion as the rate-controlling step. Paunovic, et al. [45] reported that the Ginstling-Braunshtein model provided the most accurate fit for ultrasound leaching of nickel laterite ore. This suggests that diffusion is the limiting step in the leaching process. Wang, et al. [46] employed the shrinking core model to simulate the ultrasound-assisted leaching of zinc residues. The modeling results revealed that the rate-controlling step in the leaching process was the diffusion through the product layer.

In addition, it is important to note that the ultrasound-assisted synthesis, exfoliation, and functionalization of graphene derivatives using high-grade graphite have been systematically investigated [51–56]. Li, et al. [57] calculated the selection and breakage functions of ultrasound-assisted exfoliation and breakage process of graphite oxide. They found that the breakage mechanisms of graphite oxide are attributed mainly to sheet fracture. In their study, Navik, et al. [58] proposed a cost-effective and straightforward technique to synthesize graphene from graphite in

Table 2
Main impurity element contents (the ash) of raw graphite ore (wt.%).

SiO_2	Al_2O_3	Fe_2O_3	MgO	K_2O	TiO_2	CaO
54.80	21.95	12.16	4.04	3.95	1.10	0.69

ethanol using ultrasound-assisted curcumin. This approach not only allowed for the exfoliation of graphite into graphene but also enabled the production of a graphene-curcumin hybrid, which could have potential applications in the pharmaceutical industry. In their research, Qin, et al. [59] uncovered the phenomenon of fatigue exfoliation on the graphite surface, resulting from the cyclic implosion of ultrasonic bubbles that corresponded with the ultrasound frequency. Their study demonstrated that the exfoliation rate and efficiency of the graphite layer were predominantly governed by the number of imploding bubbles situated in the effective cavitation bubble zone. Preeyanghaa, et al. [60] reported hierarchical carbon nitride (CN) nanorods displayed remarkable sonophotodegradation performance, achieving nearly 100 % degradation of Tetracycline (TC) antibiotics within 60 min under ultrasonic irradiation and visible light illumination. Moreover, the sonophotocatalytic degradation was higher than the sum of sonocatalytic and photocatalytic TC degradation using hierarchical CN nanorods due to its synergistic performance.

To our knowledge, most graphite leaching studies have focused on optimizing experimental conditions, and few studies have studied the leaching kinetics of aphanitic graphite ores to remove impurities. Meanwhile, the conventional leaching process is characterized by long reaction time, low efficiency, and high leaching agent consumption. Moreover, it is expected that ultrasound can effectively increase the leaching efficiency and the reaction rate of impurities from aphanitic graphite by decreasing the particle size, removing the passivation layer, and increasing the mass transfer rate with the help of cavitation-induced mechanical, chemical, and thermal effects. However, there is no published paper on the ultrasound-assisted removal of ash materials from aphanitic graphite from the viewpoint of leaching kinetics.

To fill this gap, this paper investigated the differences in the leaching kinetics of conventional and ultrasonic acid leaching of aphanitic graphite and revealed the relationship between ultrasound power and ultrasound-assisted leaching of aphanitic graphite. Furthermore, the enhancement mechanism of ultrasound-assisted leaching of aphanitic graphite was discussed. Finally, the future research direction for the in-depth removal of impurities from aphanitic graphite using ultrasound-assisted leaching was proposed.

2. Material and methods

2.1. Materials

Aphanitic graphite samples with 13.02 % ash content were obtained from Hunan, China. The samples were in an ultrafine size fraction (d_{50} of the samples was 3.88 μm). The fine sample used in this study was collected from the ground product of the bulk sample in a mineral processing plant. Hydrochloric acid (HCl, AR) was provided by Shanghai Aladdin Biochemical Technology Co., ltd. According to Table 2, SiO_2, Al_2O_3 and Fe_2O_3 are the main impurities.

2.2. Leaching test

To obtain a slurry with the required solid–liquid ratio and HCl concentration, pure water, raw ore sample, and hydrochloric acid were weighed and combined to yield a 150 mL mixture. The resulting slurry was placed in a 250 mL flat-bottom flask for all leaching tests. The experimental setups for both conventional and ultrasound-assisted leaching tests are illustrated in Fig. 1. For the conventional leaching test, temperature control was achieved using an HJ-2B multi-position thermostatic hotplate magnetic stirrer (Changzhou Gaode Instrument Manufacturing Co., Changzhou, China), as shown in Fig. 1(a). The magnetic stirrer bar has a 30 mm length and a 7 mm diameter. The temperature sensor was submerged in a water tank, and a magnetic stirrer bar with a length of 30 mm and diameter of 7 mm was used. Optimization of conventional leaching was conducted using a single-factor experimental design. The specific experimental conditions for each single-factor test are detailed in Table 3. For the ultrasound-assisted leaching test (Fig. 1(b)), an ultrasonic cleaner tank (Shenzhen Geneng Cleaning Equipment Co., ltd.) was utilized to control both temperature and ultrasound power, operating in a continuous mode. All ultrasound-assisted leaching tests were conducted at 8 mol/L HCl concentration and 0.1 g/L solid–liquid ratio based on the optimization results of conventional leaching.

The leaching concentrate was filtered, washed, and dried after the leaching test. The ash content determination was carried out according to Chinese Standard GB/T 3521–2008 “Method for chemical analysis of graphite” [7,61]. The ash removal rate α was calculated as follows:

$$\alpha = \frac{100^*A_F - \gamma^*A_C}{100^*A_F} \times 100, \quad (1)$$

where: γ − yield of the leaching concentrate, %; A_F − ash content of raw

Table 3
The details of experimental conditions of conventional leaching for each single-factor test.

No.	Variable	Fixed condition
(a)	HCl concentration	0.3 g/L solid–liquid ratio, 344 K temperature, 60 min leaching time, 600 r/min stirring speed
(b)	Solid-liquid ratio	8 mol/L HCl concentration, 344 K temperature, 60 min leaching time, 600 r/min stirring speed
(c)	Temperature	8 mol/L HCl concentration, 0.1 g/L solid–liquid ratio, 60 min leaching time, 600 r/min stirring speed
(d)	Leaching time	8 mol/L HCl concentration, 0.1 g/L solid–liquid ratio, 344 K temperature, 600 r/min
(e)	Stirring speed	8 mol/L HCl concentration, 0.1 g/L solid–liquid ratio, 344 K temperature, 120 min leaching time

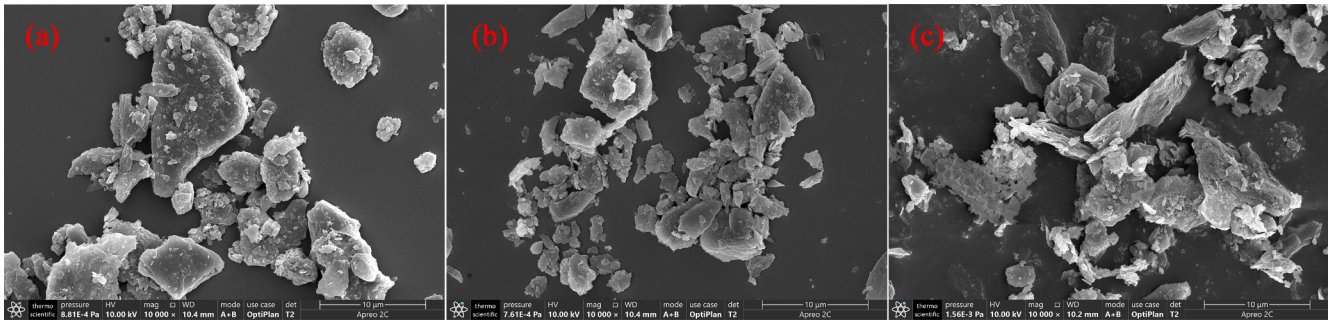

Fig. 1. The experimental apparatuses of (a) conventional and (b) ultrasound-assisted leaching tests.

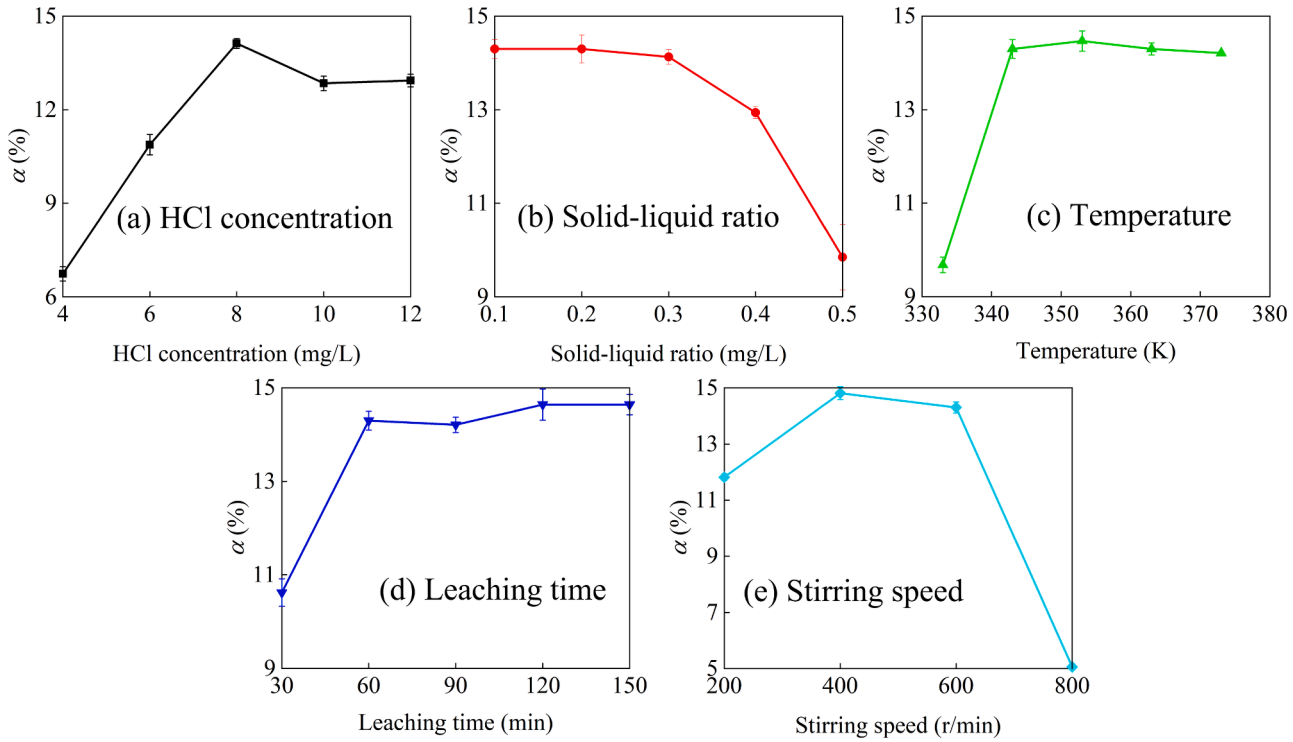

Fig. 2. Effects of different experimental parameters on ash removal rate (α) for conventional leaching.

sample, %; A_C – ash content of the leaching concentrate, %.

2.3. Characterization

The laser particle size analyzer (GSL-1000, Liaoning instrument research institute Co., ltd., China) was used to measure the particle size distribution of the graphite ore. In the laser particle size analyses, absolute ethanol (analytical reagent, Xilong Scientific Co., ltd.) was used as a solvent to avoid the agglomeration phenomenon. The detailed operating processing of the particle size measurement has been previously

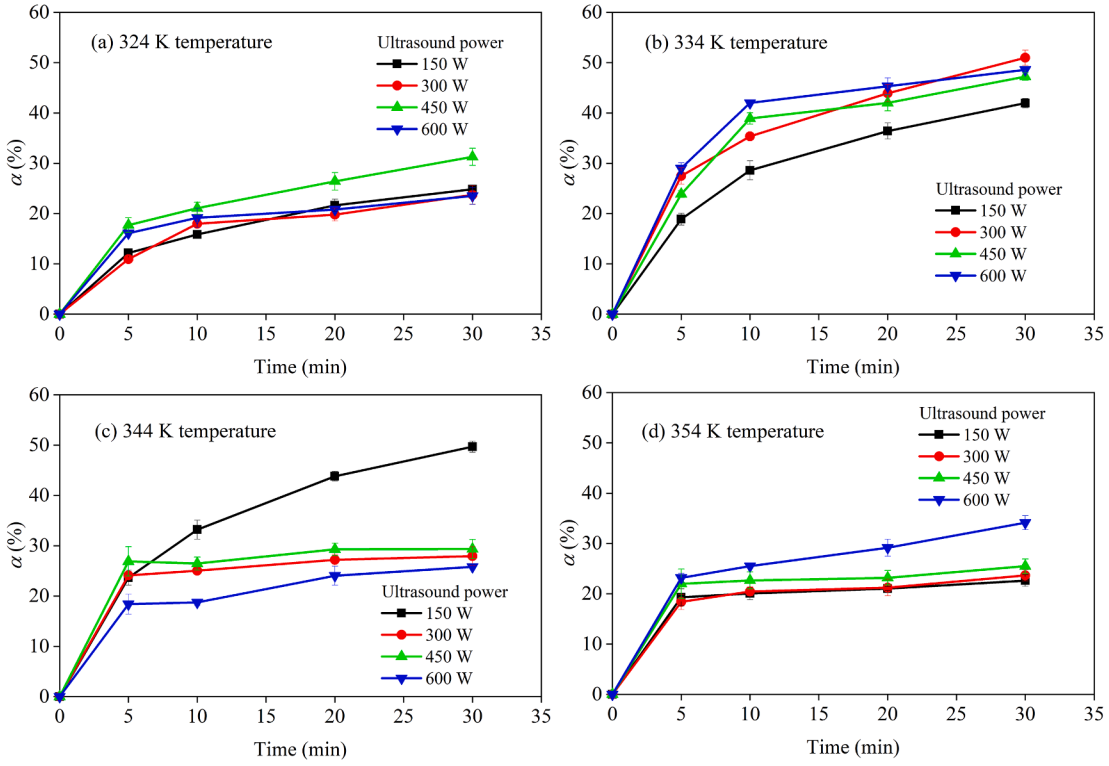

Fig. 3. Ash removal rate (α) of ultrasound leaching under different ultrasound powers and temperatures. The leaching time for ultrasound-assisted leaching refers to the ultrasonication time.

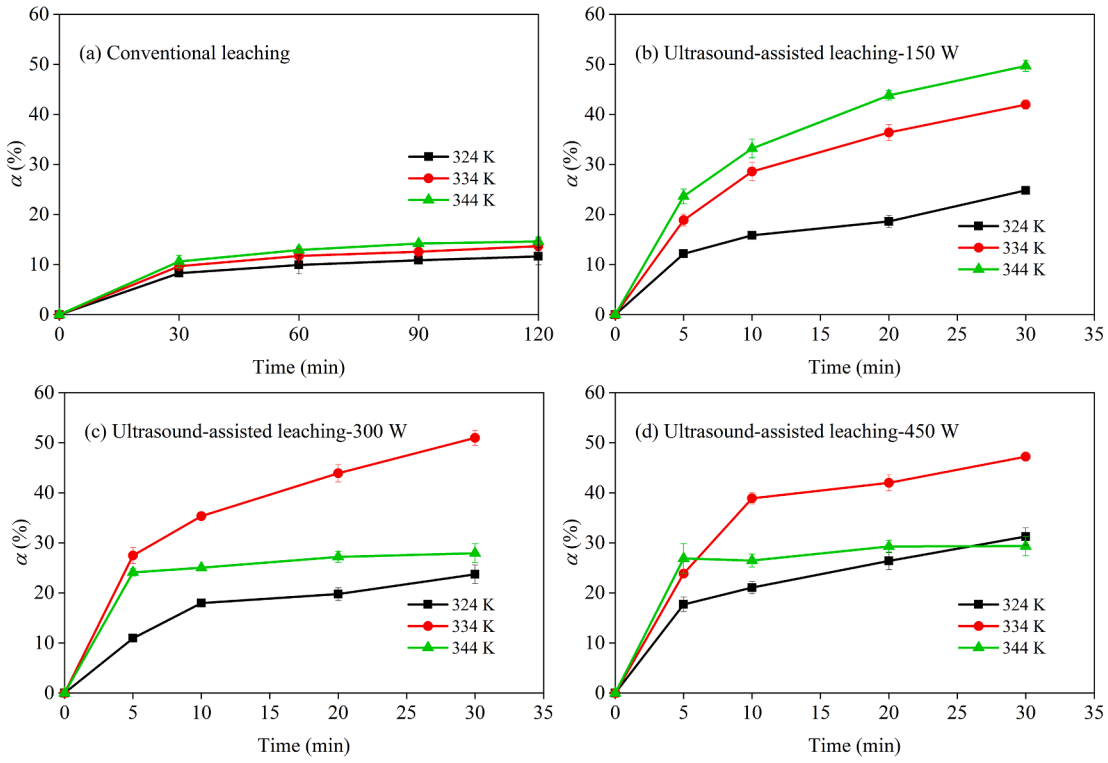

Fig. 4. Comparisons of ash removal rates for conventional and ultrasound-assisted leaching under different times.

described [5].

The chemical characterizations of raw ore and leaching concentrates were measured by XRD (6100, Shimadzu Corporation, Japan). XRD experiment was carried out at a 40 kV accelerating voltage and 30 mA current using a Cu Kα radiation source. The morphology characterizations and the impurity distribution of these samples were measured by SEM-EDS (FIB-SEM, Helios G4 CX, Thermo Fisher Scientific). The SEM and EDS images were synthesized to make the results more distinct. TEM-SEM analysis was carried out in a 200 kV transmission electron microscope (Talos F200S G2, Thermo Fischer Scientific) with a Super-X energy dispersive spectrometer system at a vacuum of 1.6×10^{-7} Pa. The detailed measurement processes of XRD, SEM-EDS, and TEM-EDS can be found in the literature [62,63].

3. Results and discussion

3.1. Effects of ultrasound power and temperature on ash removal rate α

The single-factor experimental results of conventional leaching are summarized in Fig. 2. It was found that the ash removal rate increased with increasing HCl concentration from 4 mol/L to 8 mol/L, as shown in Fig. 2a. However, the ash removal efficiency decreased under high HCl concentrations due to the high volatility of the acid. Fig. 2b indicated that there was a decrease in the ash removal efficiency with the increase in the solid–liquid ratio. On the other hand, the ash removal rate increased with increasing temperature and remained stable at approximately 14.5 % (Fig. 2c). Fig. 2d shows that a critical leaching time of 60 min was obtained for the conventional leaching with a suitable ash removal rate. It was also observed that a stirring speed of 400 rpm produced the best ash removal rate. The optimal parameters for conventional leaching were determined to be ~ 15 % ash removal rate at 8 mol/L HCl concentration, 0.1 g/L solid–liquid ratio, 344 K temperature, 400 r/min stirring speed, and 120 min leaching time, based on the results shown in Fig. 2.

Fig. 3 shows the effects of ultrasound power and temperature on the ash removal rate (α) of ultrasound leaching. As observed from Fig. 3, the α values increased with increasing leaching time. The α was approximately 50 % at 300 W ultrasound power, 334 K temperature, and 30 min leaching time. Compared to conventional leaching, ultrasound leaching can significantly increase ash removal efficiency to 50 % from 15 %. Furthermore, ultrasound leaching (30 min) resulted in a significantly shorter leaching time than conventional leaching (120 min). Thus, it was concluded that the application of ultrasound for the leaching of ash materials from graphite produced a superior ash removal efficiency than that of conventional leaching.

As observed from Fig. 3a, the α value increased with an increase in ultrasound power from 150 W to 450 W. A further increase in ultrasound power (greater than450 W) decreased the α value from ~ 30 % to ~ 20 % at a temperature of 324 K. In experiments carried out at 334 K (Fig. 3b) and 344 K (Fig. 3c), the maximum value (~50 %) was obtained at ultrasound powers of 300 W and 150 W, respectively. It is well known that the cavitation intensity increases with an increase in the ultrasound power [56,64]. With the increase in input power, the acoustic intensity increases, and the threshold of transient cavitation decreases, which leads to more cavitation bubbles collapsing [15,65]. Furthermore, the number of cavitation bubbles increases with increasing acoustic power [66]. Increased cavitation can improve the leaching process by decreasing particle size, removing inertia layers from graphite particle surfaces, generating more free radicals, and improving mass transfer. The temperature increases with ultrasound time, particularly at high power, causing a decrease in the cavitation intensity [67]. Once ultrasound power is increased to a certain value, the inhibition of cavitation phenomena results in poor ultrasound-assisted leaching efficiency.

When the temperature increased from 324 K to 334 K, the levels of α value increased from ~ 20 % to ~ 40 % (Fig. 3a and b). However, the α value decreased significantly with the further increase in the temperature from 344 K to 354 K (Fig. 3c and d). As a result of relatively high ultrasound power, the efficiency of ash removal was greatly reduced. The deteriorated phenomenon under greater temperatures can be attributed to the volatilization of HCl, resulting in a decrease in the effective concentration of HCl reacting with graphite impurity minerals. The deterioration of the cavitation intensity at a relatively high

Table 4
Leaching kinetic models.

Name		No.	Equation
Volumetric reaction model	Diffusion control	1	$-\ln(1-\alpha) = kt$
	Chemical reaction control	2	$\frac{1}{1-\alpha}-1 = kt$
Unreacted shrinkage core model	Diffusion control	3	$1-3(1-\alpha)^{2/3}+2(1-\alpha) = kt$
	Chemical reaction control	4	$1-(1-\alpha)^{1/3} = kt$

temperature is attributed to the changes in saturated vapor pressure, viscosity, and gas content [64,65,68]. Therefore, ultrasonic-assisted leaching needs to be conducted at appropriate ultrasound parameter levels, considering the effects of ultrasound power, temperature, and their interactions.

3.2. Leaching kinetics analysis of ultrasound-assisted leaching

Fig. 4 shows the experimental results at 324 K, 334 K, and 344 K temperatures with ultrasound input powers of 0 W (conventional leaching), 150 W, 300 W, and 450 W. It was directly observed that a longer leaching time of 30 min for conventional leaching was required to reach the same α level that ultrasound-assisted leaching obtained at 5 min leaching time.

Leaching kinetic models used in this study are given in Table 4. k (min^{-1}) and t (min) are reaction rate constant and leaching time, respectively. The four leaching kinetic models given in Table 4 were used to fit the experimental results of Fig. 4. The fitting performance (R^2) of different leaching kinetic models is compared in Fig. 5. It was indicated that the R^2 values under different conditions for the model 3 (unreacted shrinkage core model-diffusion control) were greater than other models. It was concluded that conventional and ultrasound-assisted leaching processes belong to diffusion control.

The activation energy of the reaction (E_a) and the pre-exponential factor (A) of the Arrhenius equation (Eq. (2)) are two important parameters to characterize the leaching kinetics of a chemical reaction process.

$$k = Ae^{-\frac{E_a}{RT}}, \quad (2)$$

where: k denotes the rate constant of the reaction, min^{-1}; R denotes a gas constant, 8.314 J/(mol·K); T denotes temperature in Kelvin, K; E_a denotes the activation energy of the chemical reaction, kJ/mol; A denotes the pre-exponential factor which, in terms of the collision theory, is the frequency of correctly oriented collisions between the reacting species.

For a good fit of a model, the coefficient of determination should be at least 0.800 [69,70]. The poor fitting performance (R^2) of these experimental data of 300 W and 450 W ultrasound powers at 344 K temperature (Fig. 5) were not used for the calculation of the equation in Eq. (2). E_a and A were estimated from the Arrhenius plot (Fig. 6). As observed from Fig. 6, ultrasound-assisted leaching had a faster reaction

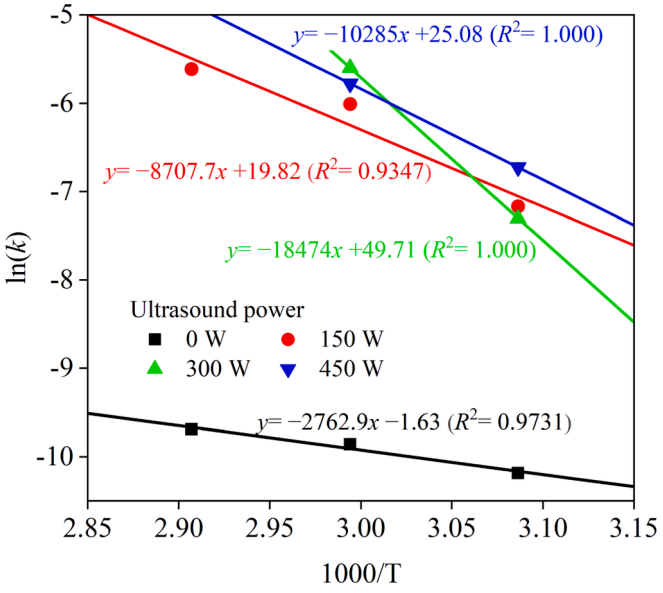

Fig. 6. Arrhenius plots of conventional (0 W) and ultrasound-assisted leaching. The solid line is the linear fitting curve.

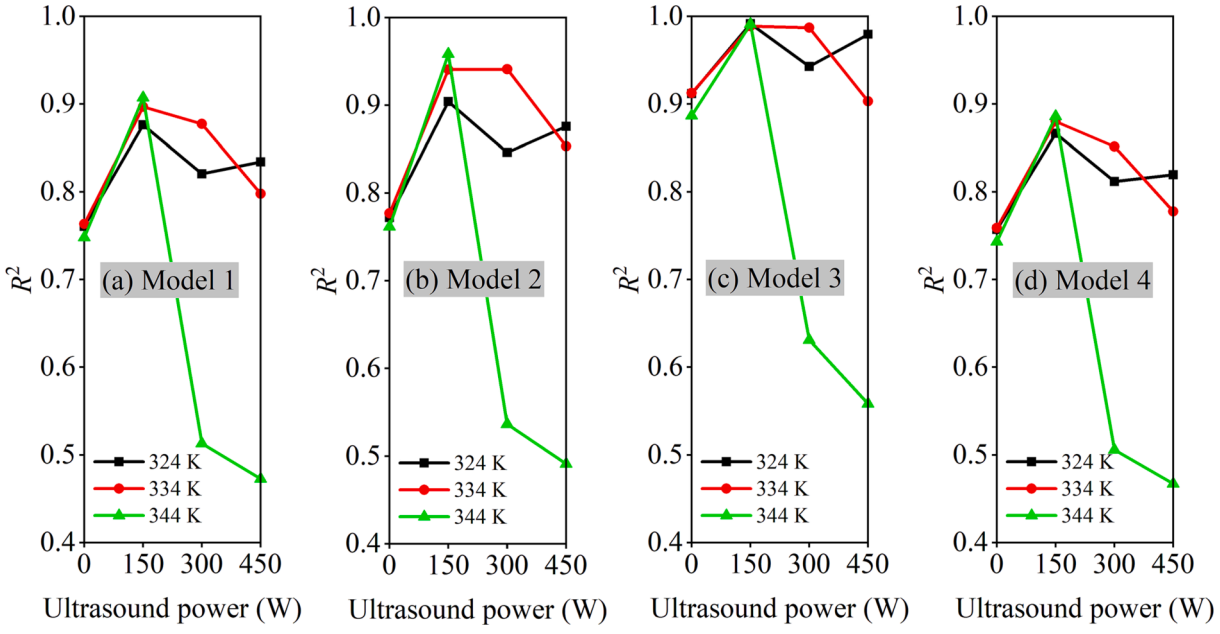

Fig. 5. Comparison of fitting performance (R^2) for conventional (0 W) and ultrasound-assisted leaching.

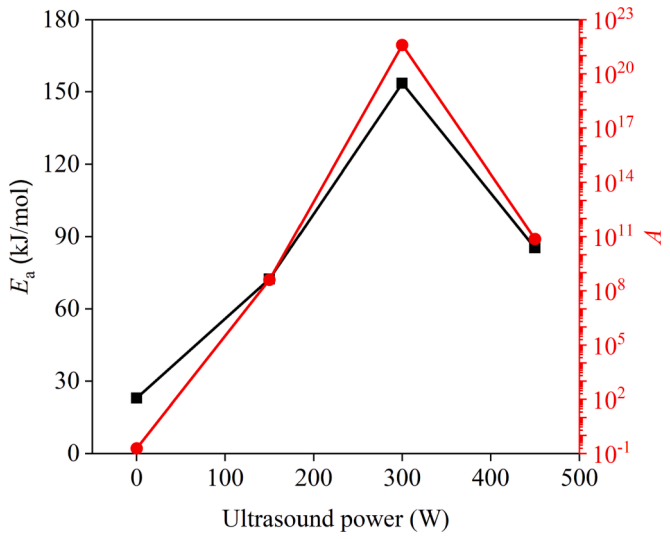

Fig. 7. Effects of ultrasound power on E_a and A.

rate constant ($6.72 \times 10^{-4} \sim 3.65 \times 10^{-3}$ min^{-1}) compared to conventional leaching ($3.77 \times 10^{-5} \sim 6.18 \times 10^{-5}$ min^{-1}). The maximum value of k 3.65×10^{-3} min^{-1} was obtained at 150 W ultrasound power at 344 K temperature.

The effects of ultrasound power on E_a and A are presented in Fig. 7. As observed from Fig. 7, the E_a value of 23 kJ/mol for conventional leaching (0 W) was significantly smaller than that of ultrasound-assisted leaching (85 ~ 154 kJ/mol). An E_a value indicates how much temperature influences a chemical reaction [71]. It can be concluded that the k value of ultrasound-assisted leaching is more dependent on the reaction temperature compared to conventional leaching. This is supported by the k values under different temperatures (Fig. 6).

Meanwhile, the A value for ultrasound-assisted leaching was a magnitude of orders greater than that of conventional leaching. As observed from the Arrhenius equation (Eq. (2), a faster k can be obtained by an increase in the A value or a decrease in the E_a value. For ultrasound-assisted leaching, several researchers have reported that the ultrasound treatment enhanced the rate constant of the chemical reaction by a significant increase in A [72–77]. Thus, the increase in the reaction rate constant for ultrasound-assisted leaching was obtained by a huge increase in A.

3.3. SEM-EDS, XRD, and TEM-SEM analysis

Fig. 8 shows the comparative results of impurity element contents and SEM images for raw ore, conventional, and ultrasound leaching concentrates. It was observed that Si was the main element for raw ore and conventional leaching concentrate (Fig. 8a & b). In addition, XRD patterns indicated that quartz was the main impurity mineral in raw ore and conventional leaching concentrate (Fig. 9). HCl leaching treatment was used to remove serpentine and clinochlore, while quartz was still present in the conventional leaching concentrate. HCl is commonly

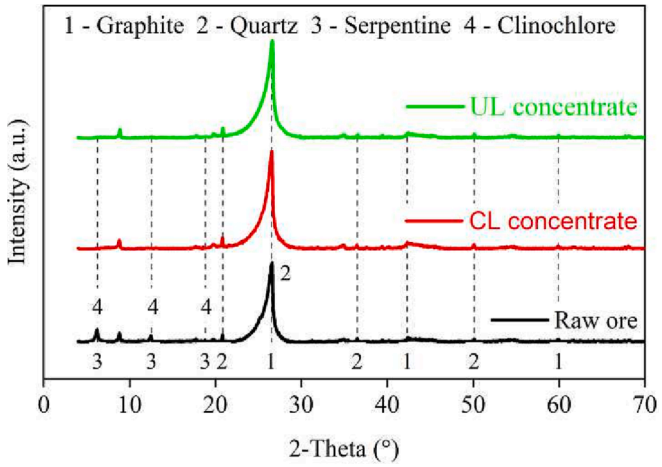

Fig. 9. XRD patterns of raw ore, CL concentrate (conventional leaching), and UL concentrate (ultrasound leaching).

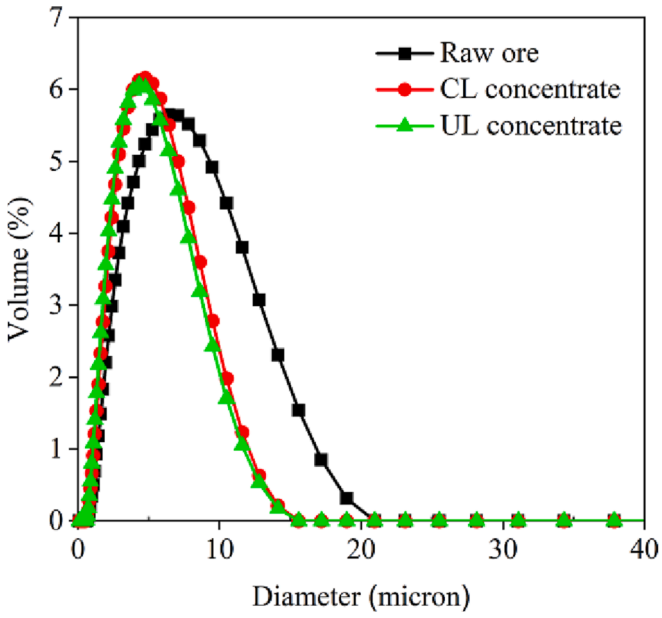

Fig. 10. Particle size distributions of raw ore, CL concentrate (conventional leaching), and UL concentrate (ultrasound leaching).

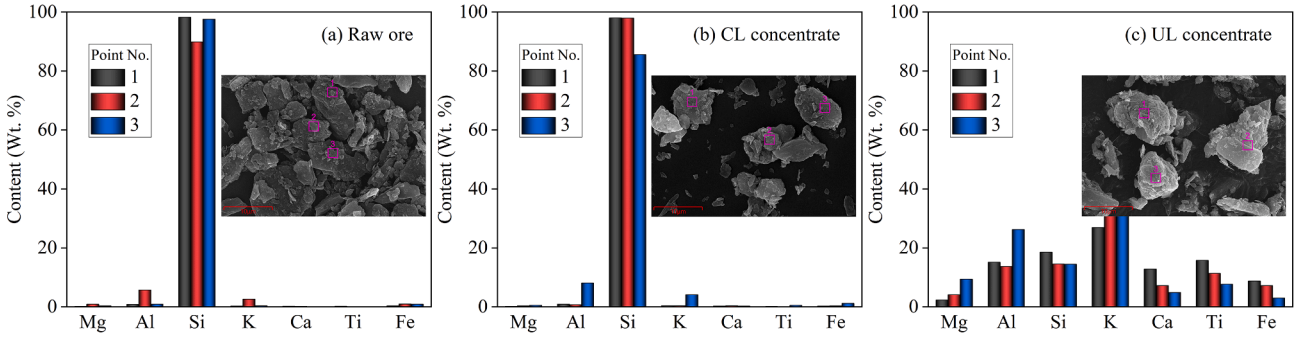

Fig. 8. Comparisons of impurity element contents and SEM images of (a) raw ore, (b) CL concentrate (conventional), and (c) UL concentrate (ultrasound).

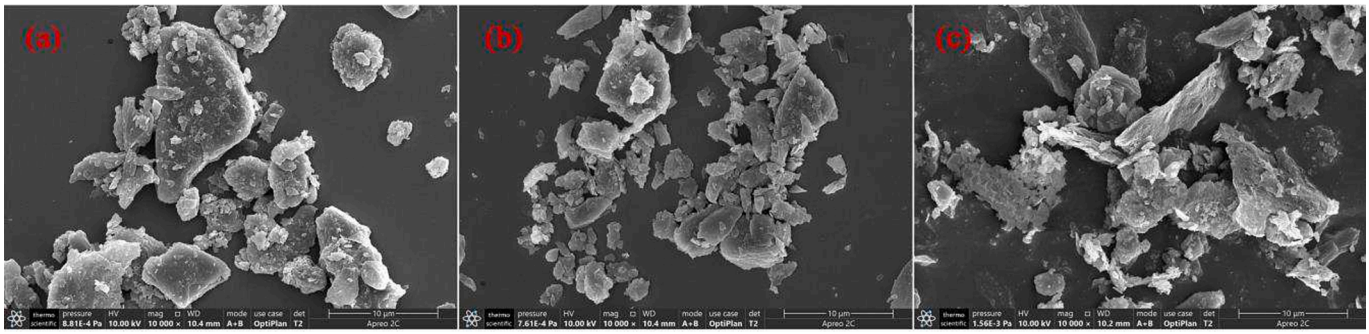

Fig. 11. SEM images of (a) raw ore, (b) CL concentrate (conventional leaching), and (c) UL concentrate (ultrasound leaching).

inefficient to remove siliceous minerals (such as quartz and clays) from graphite ores [26,27]. Quartz does not react well with HCl, while reacted clays can form inert layers (H_2SiO_3) on graphite surfaces that hinder HCl's contact and reaction with impurities. The presence of quartz and the formed inert layers lead to a low ash removal rate for conventional leaching.

As observed from Fig. 8c, the Si element content was decreased from ~ 95 % to ~ 15 %, which indicated that ultrasound treatment was useful to improve the reactivity between siliceous minerals and HCl. This indicated that ultrasound could renew the reaction surface through its ability to blow out the insoluble solid film layer on the surfaces of graphite particles. A similar phenomenon is commonly observed in processes involving ultrasound-assisted leaching [32,78–80].

Particle size distributions of raw ore, conventional, and ultrasound leaching concentrates are shown in Fig. 10. The SEM images of raw ore, conventional, and ultrasound leaching concentrates are given in Fig. 11. Compared to the raw ore and CL concentrate, the reduction in particle size of the concentrate for ultrasound-assisted leaching supported the occurrence of particle fractures, which was verified by the comparative results of SEM images in Fig. 11. As seen from Fig. 11, the particle surface of the UL concentrate was rougher than that of raw ore and CL concentrate. In addition, fine exfoliation particles were observed in the UL concentrate (Fig. 11c). Ultrasound treatment is powerful enough to overcome van der Waals forces of the graphitic materials allowing their exfoliation and dispersion into the solution [58]. Thus, the generation of a rough surface and fine exfoliation particles in the UL concentrate is attributed to the exfoliation of the layered-graphitic materials in the presence of ultrasound, which is widely applied for the graphene preparation process [51].

The reduction in particle size and the generation of the rough surface is conducive to the increases in the leaching reaction rate constant and leaching recovery, which is attributed to an increase in surface area per unit weight and the contact probability between the ash materials and the leachant [72,75,81]. The ash removal rate was kept stable at ~ 50 %, which indicated that the further improvement in the HCl leaching assisted by ultrasound may have encountered a bottleneck. The breakup of larger ore particles is an important aspect of the enhancement mechanisms of the ultrasound-assisted leaching process [32,82]. However, it is notable that there exists a concept of "critical grain size" below which the ultrasound-assisted technique is not effective for improving the leaching efficiency (45 μm for CuO) [82]. Thus, further improvement in the ash removal rate for ultrasound-assisted leaching may be limited by the critical grain size of aphanitic graphite.

The generated radicals can play a role in the leachant for the promotion of the leaching process. The temperature inside the collapsing bubbles controls the number of radicals generated. In aqueous reactions, the formation of free radicals in an acoustic field is described as follows [83]:

$$H_2O \rightarrow H^+ + OH^- \quad (3)$$

$$H^+ + H^+ \rightarrow H_2 \quad (4)$$

$$OH^- + OH^- \rightarrow H_2O_2 \quad (5)$$

$$H^+ + OH^- \rightarrow H_2O \quad (6)$$

It can be augmented by enhancing sonication power, exceeding external pressure, and reducing external (solution) temperature, leading to more radicals [68]. This is supported by the enhancement of the impurity removal reaction rate constant with the increase in the ultrasound power (Fig. 6).

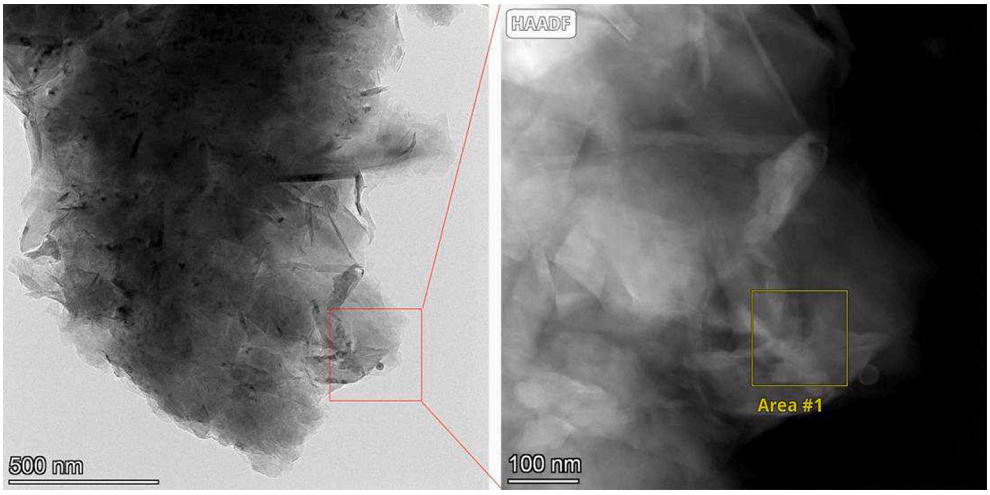

Fig. 12. TEM image of UL concentrate (ultrasound).

Graphite is a layered mineral composed of weakly bonded graphene sheets with a large aspect ratio [84]. The impurity mineral embedded in carbon layers is a nonnegligible factor for the in-depth removal of ash materials from graphite. Fig. 12 illustrates the TEM image of ultrasound leaching concentrate. As observed from Fig. 12, the flakes of graphite concentrate after ultrasound leaching were thick and had plenty of dark shadow areas between the carbon layers. These phenomena indicated the presence of impurities between carbon layers. Thus, future attention can be paid to further removing the ash materials from graphite by combining an ultrasound-assisted leaching system and some other intensity techniques such as HCl-hydrofluoric acid leaching [27,29], inorganic acid-fluoride salt leaching[30,31], and oxidation-expansion acid leaching [62,85,86].

4. Conclusions

In this study, the effects of ultrasonic power and temperature on the impurity removal rate were investigated. The following findings are highlighted:

- Ultrasonic power and temperature have a direct relation with ash removal rate.
- The unreacted shrinkage core model gave a better fit as compared to the other kinetic models.
- Ultrasonic leaching activation energy increased significantly with temperature compared to conventional leaching.
- Impurity mineral removal efficiency can be increased by destroying the inert layer on the graphite surface, promoting particle fragmentation, and generating oxidization radicals.
- The impurity mineral embedded in carbon layers cannot be completely removed by ultrasound-assisted leaching.
- Ultrasound-assisted leaching may be used in combination with another method for the deep removal of ash material.

CRediT authorship contribution statement

Xiangning Bu: Conceptualization, Software, Writing – original draft, Funding acquisition. **Zheng Tong:** Investigation, Software. **Muhammad Bilal:** Writing – review & editing, Formal analysis. **Xibing Ren:** Software, Formal analysis. **Mengqian Ni:** Investigation, Writing – review & editing, Methodology. **Chao Ni:** Validation, Supervision. **Guangyuan Xie:** Supervision.

Declaration of Competing Interest

The authors declare that they have no known competing financial interests or personal relationships that could have appeared to influence the work reported in this paper.

Data availability

Data will be made available on request.

Acknowledgement

The authors gratefully acknowledge financial support from the National Natural Science Foundation of China (Grant Nos. 52204296).

References

[1] A.D. Jara, A. Betemariam, G. Woldetinsae, J.Y. Kim, Purification, application and current market trend of natural graphite: A review, International Journal of Min. Sci. Technol. 29 (2019) 671–689.
[2] M. Govindasamy, S.-F. Wang, A. Almahri, U. Rajaji, Effects of sonochemical approach and induced contraction of core-shell bismuth sulfide/graphitic carbon nitride as an efficient electrode materials for electrocatalytic detection of antibiotic drug in foodstuffs, Ultrason. Sonochem. 72 (2021), 105445.
[3] A.A. Stewart, Graphite Statistics and Information 2023, in, National Minerals Information Center, USGS, 988 National Center Reston, VA 20192 US, 2023.
[4] Q. Yang, Y. Geng, H. Dong, J. Zhang, X. Yu, L. Sun, X. Lu, Y. Chen, Effect of environmental regulations on China's graphite export, J. Clean. Prod. 161 (2017) 327–334.
[5] X. Wang, X. Bu, C. Ni, S. Zhou, X. Yang, J. Zhang, M. Alheshibri, Y. Peng, G. Xie, Effect of scrubbing medium's particle size on scrubbing flotation performance and mineralogical characteristics of microcrystalline graphite, Miner. Eng. 163 (2021), 106766.
[6] S. Zhou, X. Wang, X. Bu, H. Shao, Y. Hu, M. Alheshibri, B. Li, C. Ni, Y. Peng, G. Xie, Effects of emulsified kerosene nanodroplets on the entrainment of gangue materials and selectivity index in aphanitic graphite flotation, Miner. Eng. 158 (2020), 106592.
[7] C. Ni, Q. Zhang, M. Jin, G. Xie, Y. Peng, H. Yu, X. Bu, Effect of high-speed shear flocculation on the flotation kinetics of ultrafine microcrystalline graphite, Powder Technol. 396 (2022) 345–353.
[8] S.C. Chelgani, M. Rudolph, R. Kratzsch, D. Sandmann, J. Gutzmer, A review of graphite beneficiation techniques, Miner. Process. Extr. Metall. Rev. 37 (2016) 58–68.
[9] S. Nazari, S. Zhou, A. Hassanzadeh, J. Li, Y. He, X. Bu, P.B. Kowalczuk, Influence of operating parameters on nanobubble-assisted flotation of graphite, J. Mater. Res. Technol. 20 (2022) 3891–3904.
[10] Y. Chen, S.C. Chelgani, X. Bu, G. Xie, Effect of the ultrasonic standing wave frequency on the attractive mineralization for fine coal particle flotation, Ultrason. Sonochem. 77 (2021), 105682.
[11] H. Chu, L. Chen, D. Lu, Y. Wang, X. Zheng, Ultrasonic pretreatment of spodumene with different size fractions and its influence on flotation, Ultrason. Sonochem. 82 (2022), 105889.
[12] L. Jin, W. Wang, Y. Tu, K. Zhang, Z. Lv, Effect of ultrasonic standing waves on flotation bubbles, Ultrason. Sonochem. 73 (2021), 105459.
[13] M. Kruszelnicki, A. Hassanzadeh, K.J. Legawiec, I. Polowczyk, P.B. Kowalczuk, Effect of ultrasound pre-treatment on carbonaceous copper-bearing shale flotation, Ultrason. Sonochem. 84 (2022), 105962.
[14] M. Zhang, Z. Xu, L. Wang, Ultrasonic treatment improves the performance of starch as depressant for hematite flotation, Ultrason. Sonochem. 82 (2022), 105877.
[15] Y. Chen, V.N. Truong, X. Bu, G. Xie, A review of effects and applications of ultrasound in mineral flotation, Ultrason. Sonochem. 60 (2020), 104739.
[16] S.D. Barma, P.K. Baskey, D.S. Rao, S.N. Sahu, Ultrasonic-assisted flotation for enhancing the recovery of flaky graphite from low-grade graphite ore, Ultrason. Sonochem. 56 (2019) 386–396.
[17] W.Z. Kang, H.J. Li, Enhancement of flaky graphite cleaning by ultrasonic treatment, R. Soc. Open Sci. 6 (2019), 191160.
[18] X. Bu, M. Alheshibri, The effect of ultrasound on bulk and surface nanobubbles: A review of the current status, Ultrason. Sonochem. 76 (2021), 105629.
[19] S. Tanaka, H. Kobayashi, S. Ohuchi, K. Terasaka, S. Fujioka, Destabilization of ultrafine bubbles in water using indirect ultrasonic irradiation, Ultrason. Sonochem. 71 (2021), 105366.
[20] T. Tuziuti, K. Yasui, W. Kanematsu, Influence of bulk nanobubble concentration on the intensity of sonoluminescence, Ultrason. Sonochem. 76 (2021), 105646.
[21] S. Zhou, S. Nazari, A. Hassanzadeh, X. Bu, C. Ni, Y. Peng, G. Xie, Y. He, The effect of preparation time and aeration rate on the properties of bulk micro-nanobubble water using hydrodynamic cavitation, Ultrason. Sonochem. 84 (2022), 105965.
[22] J. Gao, X. Bu, S. Zhou, X. Wang, M. Alheshibri, Y. Peng, G. Xie, Graphite flotation by β-cyclodextrin/kerosene Pickering emulsion as a novel collector, Miner. Eng. 178 (2022), 107412.
[23] X. Bu, T. Zhang, Y. Peng, G. Xie, E. Wu, Multi-stage flotation for the removal of ash from fine graphite using mechanical and centrifugal forces, Minerals 8 (2018) 15.
[24] X. Wang, Purification study of a cryptocrystalline graphite ore from Fujian Province (in Chinese), Modern Mining 34 (2018) 157–158.
[25] C.-Q. Liu, X. Gao, Experimental study on aphanitic graphite purification with acid and alkali method, Coal Technology 34 (2015) 329–331, in Chinese.
[26] H. Wang, Q. Feng, X. Tang, K. Liu, Preparation of high-purity graphite from a fine microcrystalline graphite concentrate: Effect of alkali roasting pre-treatment and acid leaching process, Sep. Sci. Technol. 51 (2016) 2465–2472.
[27] Ö. Kaya, M. Canbazoğlu, Chemical demineralization of three different graphite ores from Turkey, Mining, Metallurgy & Exploration 26 (2009) 158–162.
[28] Q. Hong, Y. He, H. Liu, L. Shi, X. Xia, Investigations on electrochemical performances of purified natural microcrystalline graphite (in Chinese), Non-Metallic Mines, 33 (2010) 45-48, 51.
[29] W. Tang, J. Kuang, W. Xie, H. Xu, B. Deng, C. Long, The effect of mixed-acid purification on the fixed carbon content of aphanitic graphite (in Chinese), Carbon Techniques 32 (2013) A9–A12.
[30] K. Zaghib, X. Song, A. Guerfi, R. Rioux, K. Kinoshita, Purification process of natural graphite as anode for Li-ion batteries: chemical versus thermal, J. Power Sources 119–121 (2003) 8–15.
[31] W. Xie, Z. Wang, J. Kuang, H. Xu, S. Yi, Y. Deng, T. Cao, Z. Guo, Fixed carbon content and reaction mechanism of natural microcrystalline graphite purified by hydrochloric acid and sodium fluoride, Int. J. Miner. Process. 155 (2016) 45–54.
[32] X. Bu, J.K. Danstan, A. Hassanzadeh, A. Behrad Vakylabad, S.C. Chelgani, Metal extraction from ores and waste materials by ultrasound-assisted leaching -an overview, Miner. Process. Extr. Metall. Rev. (2022) 1–18.
[33] K.M. Swamy, K.L. Narayana, Chapter 4 Ultrasound-assisted leaching, in: L. de Castro, F.P. Capote (Eds.), Techniques and instrumentation in Analytical Chemistry, Elsevier, Amsterdam, 2007, pp. 99–142.
[34] S. Vyas, Y.-P. Ting, A Review of the Application of Ultrasound in Bioleaching and Insights from Sonication in (Bio)Chemical Processes, Resources 7 (2018) 3.

[35] K.M. Swamy, K. Sarveswara Rao, K.L. Narayana, J.S. Murty, H.S. Ray, Application of Ultrasound in Leaching, Miner. Process. Extr. Metall. Rev. 14 (1995) 179–192.
[36] H. Srivalli, R. Nagarajan, Mechanistic study of ultrasound-assisted solvent leaching of sodium and potassium from an Indian coal using continuous and pulsed modes of operation, Chem. Eng. Commun. 206 (2019) 207–226.
[37] G. Rahimi, S.O. Rastegar, F. Rahmani Chianeh, T. Gu, Ultrasound-assisted leaching of vanadium from fly ash using lemon juice organic acids, RSC Advances 10 (2020) 1685–1696.
[38] M.D. Turan, Z.A. Sari, A. Demiraslan, Ultrasound-assisted leaching and kinetic study of blended copper slag, Metall. Mater. Trans. B-Proc. Metall. Mater, Proc. Sci. 50 (2019) 1949–1956.
[39] X. Li, P. Xing, X. Du, S. Gao, C. Chen, Influencing factors and kinetics analysis on the leaching of iron from boron carbide waste-scrap with ultrasound-assisted method, Ultrason. Sonochem. 38 (2017) 84–91.
[40] Y.-F. Zhang, J. Ma, Y.-H. Qin, J.-F. Zhou, L. Yang, Z.-K. Wu, T.-L. Wang, W.-G. Wang, C.-W. Wang, Ultrasound-assisted leaching of potassium from phosphorus-potassium associated ore, Hydrometall. 166 (2016) 237–242.
[41] B. Avvaru, S.B. Roy, S. Chowdhury, K.N. Hareendran, A.B. Pandit, Enhancement of the Leaching Rate of Uranium in the Presence of Ultrasound, Ind. Eng. Chem. Res. 45 (2006) 7639–7648.
[42] H. He, J. Cao, N. Duan, Ultrasound and mechanical activation cleaner promote lattice manganese extraction: A combined experimental and modeling study, J. Clean. Prod. 143 (2017) 231–237.
[43] Q. Gui, M.I. Khan, S. Wang, L. Zhang, The ultrasound leaching kinetics of gold in the thiosulfate leaching process catalysed by cobalt ammonia, Hydrometall. 196 (2020), 105426.
[44] J. Ma, Y. Zhang, Y. Qin, Z. Wu, T. Wang, C. Wang, The leaching kinetics of K-feldspar in sulfuric acid with the aid of ultrasound, Ultrason. Sonochem. 35 (2017) 304–312.
[45] P. Paunovic, G. Nacevski, A. Petrovski, A. Tomova, A. Grozdanov, A. Dimitrov, Kinetic analysis of ultrasound leaching of nickel laterite ore, Bul. Chem. Commun. 51 (2019) 12–18.
[46] X. Wang, C. Srinivasakannan, X.-H. Duan, J.-H. Peng, D.-J. Yang, s.-h. Ju, Leaching kinetics of zinc residues augmented with ultrasound, Sep. Purif. Technol. 115 (2013) 66–72.
[47] S.D. Barma, R. Sathish, P.K. Baskey, Ultrasonic-assisted cleaning of Indian low-grade coal for clean and sustainable energy, J. Clean. Prod. 195 (2018) 1203–1213.
[48] B. Ambedkar, R. Nagarajan, S. Jayanti, Ultrasonic coal-wash for de-sulfurization, Ultrason. Sonochem. 18 (2011) 718–726.
[49] S. Balakrishnan, V.M. Reddy, R. Nagarajan, Ultrasonic coal washing to leach alkali elements from coals, Ultrason. Sonochem. 27 (2015) 235–240.
[50] S. Lahiri, R.L. Bhardwaj, D. Mandal, P.R. Gogate, Intensified dissolution of uranium from graphite substrate using ultrasound, Ultrason. Sonochem. 65 (2020), 105066.
[51] K. Muthoosamy, S. Manickam, State of the art and recent advances in the ultrasound-assisted synthesis, exfoliation and functionalization of graphene derivatives, Ultrason. Sonochem. 39 (2017) 478–493.
[52] S. Shi, R. Zhong, L. Li, C. Wan, C. Wu, Ultrasound-assisted synthesis of graphene@MXene hybrid: A novel and promising material for electrochemical sensing, Ultrason. Sonochem. 90 (2022), 106208.
[53] Z. Wang, H. Zhou, J. Xue, X. Liu, S. Liu, X. Li, D. He, Ultrasonic-assisted hydrothermal synthesis of cobalt oxide/nitrogen-doped graphene oxide hybrid as oxygen reduction reaction catalyst for Al-air battery, Ultrason. Sonochem. 72 (2021), 105457.
[54] Y. Yan, S. Manickam, E. Lester, T. Wu, C.H. Pang, Synthesis of graphene oxide and graphene quantum dots from miscanthus via ultrasound-assisted mechano-chemical cracking method, Ultrason. Sonochem. 73 (2021), 105519.
[55] Y. Yu, J. Wang, Preparation of graphene/PMMA composites with assistance of ultrasonic wave under supercritical CO2 conditions, Ultrason. Sonochem. 73 (2021), 105487.
[56] A. Ručigaj, J.G. Connell, M. Dular, B. Genorio, Influence of the ultrasound cavitation intensity on reduced graphene oxide functionalization, Ultrason. Sonochem. 90 (2022), 106212.
[57] C. Li, J. Lin, L. Shen, N. Bao, Quantitative analysis and kinetic modeling of ultrasound-assisted exfoliation and breakage process of graphite oxide, Chem. Eng. Sci. 213 (2020), 115414.
[58] R. Navik, Y. Gai, W. Wang, Y. Zhao, Curcumin-assisted ultrasound exfoliation of graphite to graphene in ethanol, Ultrason. Sonochem. 48 (2018) 96–102.
[59] L. Qin, B.M. Maciejewska, T. Subroto, J.A. Morton, K. Porfyrakis, I. Tzanakis, D. G. Eskin, N. Grobert, K. Fezzaa, J. Mi, Ultrafast synchrotron X-ray imaging and multiphysics modelling of liquid phase fatigue exfoliation of graphite under ultrasound, Carbon 186 (2022) 227–237.
[60] M. Preeyanghaa, V. Vinesh, B. Neppolian, Complete removal of Tetracycline by sonophotocatalysis using ultrasound-assisted hierarchical graphitic carbon nitride nanorods with carbon vacancies, Chemosphere 287 (2022), 132379.
[61] Z. Tong, L. Liu, Z. Yuan, J. Liu, J. Lu, L. Li, The effect of comminution on surface roughness and wettability of graphite particles and their relation with flotation, Miner. Eng. 169 (2021), 106959.
[62] Y. Chen, P. Li, X. Bu, L. Wang, X. Liang, S. Chehreh Chelgani, In-depth purification of spent pot-lining by oxidation-expansion acid leaching – A comparative study, Sep. Purif. Technol. 303 (2022), 122313.
[63] X. Bu, G. Evans, G. Xie, Y. Peng, Z. Zhang, C. Ni, L. Ge, Removal of fine quartz from coal-series kaolin by flotation, Appl. Clay. Sci. 143 (2017) 437–444.
[64] K. Yasui, Acoustic cavitation and bubble dynamics, Springer International Publishing, Cham, Switzerland, 2018.
[65] H. Xu, J. Tu, F. Niu, P. Yang, Cavitation dose in an ultrasonic cleaner and its dependence on experimental parameters, Appl. Acoust. 101 (2016) 179–184.
[66] A. Brotchie, F. Grieser, M. Ashokkumar, Effect of Power and Frequency on Bubble-Size Distributions in Acoustic Cavitation, Phys. Rev. Lett. 102 (2009), 084302.
[67] N.V. Dezhkunov, A. Francescutto, P. Ciuti, F. Sturman, Temperature dependence of cavitation activity at different ultrasound intensities, in: XVI Session of the Russian Acoustical Society, Moscow, 2005, pp. 74–77.
[68] S. Kentish, M. Ashokkumar, The physical and chemical effects of ultrasound, in: H. Feng, G. Barbosa-Canovas, J. Weiss (Eds.), Ultrasound Technologies for Food and Bioprocessing, Springer New York, New York, NY, 2011, pp. 1–12.
[69] X. Bu, G. Xie, Y. Peng, Y. Chen, Kinetic modeling and optimization of flotation process in a cyclonic microbubble flotation column using composite central design methodology, Int. J. Miner. Process. 157 (2016) 175–183.
[70] A.M. Joglekar, A.T. May, Product excellence through design of experiments, Cereal Foods World 32 (1987) 857.
[71] Z.-D. He, Y.-X. Chen, E. Santos, W. Schmickler, The Pre-exponential Factor in Electrochemistry, Angew. Chem.-Int. Edit. 57 (2018) 7948–7956.
[72] A.K. Mesci, F. Sevim, Dissolution of magnesia in aqueous carbon dioxide by ultrasound, Int. J. Miner. Process. 79 (2006) 83–88.
[73] C. Horst, Y.S. Chen, U. Kunz, U. Hoffmann, Design, modeling and performance of a novel sonochemical reactor for heterogeneous reactions, Chem. Eng. Sci. 51 (1996) 1837–1846.
[74] J. Wang, F. Faraji, A. Ghahreman, Effect of Ultrasound on the Oxidative Copper Leaching from Chalcopyrite in Acidic Ferric Sulfate Media, Minerals 10 (2020) 633.
[75] T. Ingeç, T. Tekin, Effect of Ultrasound on the Production Reaction Kinetics of Sodium Thiosulfate, Chem. Eng. Technol. 27 (2004) 150–153.
[76] T. Tekin, D. Tekin, M. Bayramoğlu, Effect of ultrasound on the dissolution kinetics of phosphate rock in HNO3, Ultrason. Sonochem. 8 (2001) 373–377.
[77] F. Ferrero, M. Periolatto, Ultrasound for low temperature dyeing of wool with acid dye, Ultrason. Sonochem. 19 (2012) 601–606.
[78] O. Johansson, T. Pamidi, V. Shankar, Extraction of tungsten from scheelite using hydrodynamic and acoustic cavitation, Ultrason. Sonochem. 71 (2021), 105408.
[79] H.W. Lee, N.W. Kim, W.H. Nam, Y.S. Lim, Sonochemical activation in aqueous medium for solid-state synthesis of BaTiO3 powders, Ultrason. Sonochem. 82 (2022), 105874.
[80] Z. Sharifzadeh, K. Berijani, A. Morsali, High performance of ultrasonic-assisted synthesis of two spherical polymers for enantioselective catalysis, Ultrason. Sonochem. 73 (2021), 105499.
[81] X. Wang, D.-J. Yang, C. Srinivasakannan, J.-H. Peng, X.-H. Duan, S.-H. Ju, A comparison of the conventional and ultrasound-augmented leaching of zinc residue using sulphuric acid, Arab. J. Sci. Eng. 39 (2014) 163–173.
[82] K.M. Swamy, K.L. Narayana, Ultrasonically assisted leaching, in: T.J. Mason, A. Tiehm (Eds.), Advances in Sonochemistry, JAI Press, Tokyo, Japan, 2001.
[83] L.H. Thompson, L.K. Doraiswamy, Sonochemistry: Science and Engineering, Ind. Eng. Chem. Res. 38 (1999) 1215–1249.
[84] Q. Tang, J. Wu, H. Sun, S. Fang, Crystallization degree change of expanded graphite by milling and annealing, J. Alloy. Compd. 475 (2009) 429–433.
[85] J. Kim, B. Kim, Chemical and low-expansion treatments for purifying natural graphite powder, Physicochem. Probl. Miner. Process. 41 (2007) 37–49.
[86] B.G. Kim, S.K. Choi, C.L. Park, H.S. Chung, H.S. Jeon, Inclusion of Gangue Mineral and Its Mechanical Separation from Expanded Graphite, Part. Sci. Technol. 21 (2003) 341–351.